Domain-period method for determination of the energy of the Dzyaloshinskii-Moriya interaction in [Co/Pd(111)]₅ superlattices

A. G. Kozlov [1], A. G. Kolesnikov [1], M. E. Stebliy,[1] A. P. Golikov,[2] and A. V. Davydenko [1,*]

[1]*Laboratory of Thin Film Technologies, School of Natural Sciences, Far Eastern Federal University, Vladivostok 690950, Russian Federation*
[2]*Institute of Chemistry FEB RAS, Vladivostok 690022, Russian Federation*

Determination of the energy of the interface Dzyaloshinskii-Moriya interaction (DMI) along with a definition of the basic magnetic characteristics in ferromagnetic/nonmagnetic multilayered systems are both required for the construction of a magnetic skyrmion recording medium. A method for estimating the energy of the effective DMI, which compares the periods of micromagnetically simulated and experimentally measured demagnetized domain structures, is widely used for investigations of heavy metal/ferromagnetic superlattices. In the present paper, the applicability of this method was tested on a series of symmetric epitaxial [Co/Pd(111)]₅ superlattices with Co layers of varying thickness. We examined the problem of ambiguous determination of the DMI energy, which is related to the dependence of the periodicity of the domain structure, experimentally measured in a sample on the direction of a demagnetizing field. The Co thickness dependencies of the effective and surface DMI constants, obtained using in-plane and out-of-plane demagnetized structures and fixed micromagnetic parameters, were qualitatively and quantitatively different. Having analyzed the Co thickness dependencies of the DMI energies in the entire series of samples, we found that the DMI energies obtained using in-plane rather than out-of-plane demagnetized domain structures are more acceptable. Of greatest importance for the accurate determination of the DMI energy in an investigated system is the knowledge of the exchange interaction constant. The applicability of the method in the case of variable micromagnetic parameters and the reliability of the results obtained from the samples with different magnetic parameters are discussed.

I. INTRODUCTION

The Dzyaloshinskii-Moriya interaction (DMI) became one of the most intriguing phenomena in modern nanomagnetism. The necessary conditions for the existence of DMI in materials are strong spin-orbit coupling and a lack of inversion symmetry [1,2]. These requirements may be fulfilled in the interfaces between ferromagnetic (FM) and nonmagnetic (NM) layers. Hence, interface DMI may be stabilized in ultrathin NM/FM/NM structures [3,4]. It was reported that the DMI is rather strong at the interfaces between FM and heavy metals (HMs) due to strong spin-orbit coupling in HMs [5]. Additive DMI may be obtained in the HM1/FM/HM2 systems with an appropriate choice of HM layers [6,7]. Strong interface DMI with perpendicular magnetic anisotropy (PMA) stabilize homochiral Néel domain walls (DWs) [8] and Néel skyrmions [9] which may be efficiently displaced by current pulses due to the spin-orbit torque (SOT) effect [10]. Different concepts of racetrack memories based on DWs and skyrmions have already been introduced [11,12]. An important step towards working racetrack memory was switching researchers' attention to multilayered structures or superlattices [HM1/FM/HM2]ₙ [6,7]. On the one hand, PMA and DMI are conserved in such magnetic superlattices due to a large number of interfaces. On the other hand, the overall thickness of the structures may be sufficiently increased which makes the skyrmions thermally stable. Moreover, growing dipolar interaction demagnetizes the structures and facilitates the formation of skyrmions.

Construction of the chiral magnetic systems with the required characteristics implies knowledge of the energy of the DMI. Different methods and approaches are used for the measurement of DMI energy. The first method is Brillouin light spectroscopy which directly determines the effective DMI energy by measuring the frequency difference between negative (Stokes) and positive (anti-Stokes) spin-wave frequencies in Damon-Eshbach geometry [3,4,13]. This method is quite reliable, but the measurements are time-consuming. It is worth noting that light falling at nonzero angles to a metal surface only penetrates depths comparable with a skin depth for light in metals (several tenths of nanometers) [14]. The thickness of superlattices may be larger, hence the information given by Brillouin light spectroscopy may only refer to the top layers of the structures. The second method is based on the asymmetrical propagation of chiral Néel DWs under the influence of in-plane (IP) and out-of-plane (OOP) magnetic fields [15,16]. Later, it was shown that the definition of the effective DMI energy by this method in a creep regime is not straightforward, and one needs to take into account the antisymmetric contribution [17,18] or work in a flow regime with extremely high velocities [19]. This method is suited for systems with large energies of PMA and isolated domains, but it does not work in systems with labyrinth domain structures.

*avdavydenko@gmail.com

There are also various other schemes for measuring DMI: DW propagation via the SOT effect in the presence of IP magnetic fields [20], magnetic droplet nucleation [21], and investigating the microstructure of DWs in combination with micromagnetic modeling [22]. These methods either have insufficient accuracy or are not applicable in the case of a spin spiral magnetic state.

Under these circumstances, a method based on the comparison of the periods of experimentally measured labyrinth structures with micromagnetically simulated ones seems to be straightforward [6,10]. It only needs knowledge of macroscopic magnetic parameters, which can be measured or found in the literature, and demagnetized domain structures, which may be obtained by various experimental schemes. Moreover, a two-dimensional (2D) [23] and an explicit three-dimensional (3D) [24] analytical model for calculating DMI have been introduced. The 2D analytical model did not take into account the possible z dependence of the layers' magnetic structure. It was shown that dipolar interlayer interaction in multilayered structures may lead to the existence of hybrid chiral DWs [25,26]. The competition between interlayer dipolar and DMI interactions leads to flux-closured DWs configurations which have a completely different energy when compared with the energies of DWs with a fixed internal magnetic structure. Therefore, using the 3D analytical model, in which each layer of the multilayered structure is described by its wall angle ψ_i, is preferable.

In spite of the relative simplicity of the periodicity analysis method, there are some problems of its implementation. The main problem is related with the choice of an experimental demagnetization procedure. The period of a demagnetized structure quite strongly depends on the direction of the demagnetizing field. Generally, the periodicity of the OOP demagnetized structures is larger than IP demagnetized ones by a factor of 1.2–1.5 [25,27]. Such uncertainty introduces a significant spreading of the results. In some papers IP demagnetized structures were used [25,28] while in other papers OOP demagnetized structures were considered [6,7,29–31]. Therefore, one needs to determine which experimentally demagnetized state is the ground state. The first problem gives rise to the second one which is related with the applicability of the method to the structures which do not self-demagnetize and may stay in a metastable monodomain state with the magnetization aligned parallel to the easy axis. In most of the papers using micromagnetic simulations to obtain an equilibrium magnetic state, a random initial magnetic state was used [6,7,28,30]. Relaxation from the random magnetic state leads to the existence of a large number of skyrmions in the relaxed magnetic structure which often does not coincide with experimental labyrinth magnetic state and hence may not be the ground state. The effect of the uncertainty of the magnetic parameters on the result should be taken into account.

In the present paper, we consider the aforementioned problems by testing the domain-period method for determining the energy of DMI in [Co(d_{Co})/Pd]₅ superlattices with Co layers of different thicknesses. The existence of strong DMI in the symmetric [Co/Pd]₅ system may be explained by an unequal lattice distortion in the bottom Pd/Co and top Co/Pd interfaces, which breaks the symmetry of the system. Moreover, strong DMI was experimentally measured in polycrystalline [Co/Pd]$_N$ superlattices [32]. A comprehensive analysis of the investigated system allows us to obtain reliable results which are compared with our previous investigation of DMI in the [Co/Pd]$_N$ superlattices with different numbers of Co/Pd bilayers [33].

II. EXPERIMENTAL DETAILS AND METHODS

The superlattices were grown in a molecular-beam epitaxy chamber with a base pressure of 3×10^{-10} Torr. Si(111) wafers misoriented towards [112] by 0.1° were used as substrates. Wafers were cut into 4 mm × 13 mm pieces, cleaned by acetone, isopropyl, and deionized water in an ultrasonic bath, then dried and loaded in the vacuum chamber. After indirect heating at a temperature of 500 °C, the substrates were flash-heated several times by direct current at 1200 °C by and then cooled down to near room temperature. The rates of growth for Cu, Co, and Pd were 0.9, 0.22, and 0.2 nm/min, respectively. The rates of deposition were monitored by a quartz crystal microbalance. The temperature of the substrates was varied from 75 °C during the deposition of the Cu buffer layer, to 110 °C during the deposition of the top Co and Pd layers. Changes in the temperature of the samples during the deposition of different materials were caused by the different radiative heating of the samples from the effusion cells. Epitaxial [Co(d_{Co} nm)/Pd(2 nm)]₅ superlattices were grown on a Si(111)/Cu(2 nm)/Pd(3 nm) surface. A Cu(2 nm) buffer layer was formed on a Si(111) substrate to prevent the intermixing of Pd and Si and to initiate epitaxial growth of fcc Pd(111). The thickness of the cap Pd layer was 3 nm, which is sufficient to prevent oxidization of the structure. We chose the number of Co/Pd bilayers to be equal to 5 to consider maximum variety of magnetic configurations of the investigated superlattices: from the samples stable in monodomain state with rectangular OOP hysteresis loops to the self-demagnetizing samples. The thickness of the Co layers d_{Co} was varied between 0.6 and 5 nm. In the following text, a superlattice with a given thickness of Co, for example, 1.2 nm, will be denoted as Co(1.2).

The growth processes and roughness were investigated *in situ* using a scanning tunneling microscope (STM) manufactured by Omicron. The lattice period of the metal layers during growth and their structure were analyzed using reflection high-energy electron diffraction (RHEED), made by Staib Instruments. RHEED measurements were done simultaneously with the deposition of the samples. Magnetic characterization of the samples was carried out using a vibrating sample magnetometer (VSM), with magnetic fields up to 27 kOe, manufactured by Lakeshore. The magnetic structure was measured by a magnetic-force microscope (MFM) developed by NT-MDT. MFM images were obtained in the switched-off feedback loop mode using MFM-HM tips manufactured by NT-MDT. The typical distance between the sample surface and magnetic tip was 50 nm.

Micromagnetic simulations were carried out using MU-MAX3 software [34]. We used both accurate and single z-cell effective models. All the layers were set explicitly in the accurate model, except in the Co(1.4) samples where the thickness of the Pd layers was taken as 2.1 nm in order to fit the simulation grid. The effective model implies that all

the magnetic parameters of each FM layer are averaged in a certain way over the whole FM + NM period [10]. Therefore, one micromagnetic cell corresponds to one FM/NM bilayer, and N cells are needed to model the [FM/NM]$_N$ multilayered structure in the z direction. In this case economy of the time of calculations in not significant, because usually the thickness of a FM layer is less than the thickness of a NM layer, and the number of magnetic cells remains the same as in the case of the accurate model. To go further, one may combine all repetitions and describe the entire [FM/NM]$_N$ structure by one cell in the z direction. The size of the cell in the z direction has to be the size of the cell for one FM/NM period multiplied by the number of FM/NM bilayers. Using the single z-cell effective model significantly speeds up the calculations. The lateral sizes of the simulation areas were 2 μm × 2 μm for the calculation of the domain structures [6 μm × 6 μm and 4 μm × 4 μm in the case of Co(0.8) and Co(1) superlattices, respectively] and 1 μm × 1 μm [2 μm × 2 μm in the case of Co(0.8) and Co(1) superlattices] for the calculation of the hysteresis loops. The lateral cell size was 2 nm × 2 nm. The cell size in the accurate model in the direction of the normal to the surface was varied to fit the simulation grid defined by thickness of the layers, but never exceeded the thickness of the Co layers. Two-dimensional periodic boundary conditions with ten repetitions in lateral directions were used in the modeling. The total energy of the system was minimized by the steepest descent method, with the built-in function MINIMIZE(). The RELAX() function was used in the calculations from the initial

random magnetic state. The stopping criterion for energy minimization, MINIMIZERSTOP, was set to 5×10^{-5}. The saturation magnetization and energies of PMA were determined from the experiment. The basic considered value of the exchange constant was 25 pJ/m because using this value in the previous paper [33] led to the best coincidence between the simulations and the experiment. The variation of the results depending on the small deviation of the micromagnetic parameters from the basic values is also considered. Periodicities of the domains in the ground state were also calculated analytically using 2D [23] and 3D [24] models.

III. RESULTS AND DISCUSSION

A. Structural characterization

Epitaxial growth in this system is confirmed by RHEED. RHEED streaks are observed in all samples during the growth of [Co(d_{Co})/Pd(2 nm)]$_5$ structures. The RHEED pattern of the Si(111)/Cu(2 nm)/Pd(3 nm)/Co(1 nm) surface is shown in Fig. 1(a), as an example. The structure and growth processes of the crystalline [Co(d_{Co})/Pd(2 nm)]$_5$ superlattices are similar to those for [Co/Pd(111)]$_N$ superlattices, which were thoroughly described in our previous paper [33]. In this section we focus on strain relaxation in the Co layers which depends on the Co thickness. The bulk lattice parameters of fcc-Pd and fcc-Co are 0.389 and 0.355 nm, respectively. Hence, Co is largely (9.6%) strained when deposited on the Pd surface. The growth of Co on the Pd(111) surface is incoherent
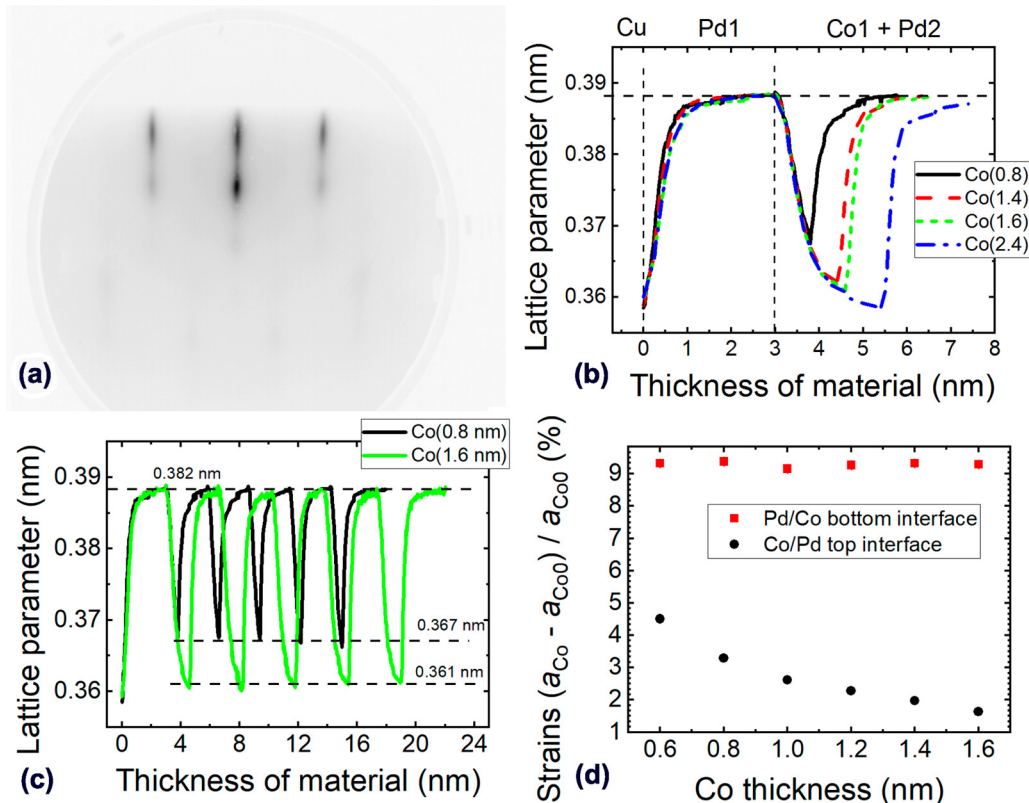

FIG. 1. (a) RHEED pattern of the Si(111)/Cu(2 nm)/Pd(3 nm)/Co(1 nm) surface. (b) Lattice parameter in the first three material layers of the different [Co(d_{Co})/Pd(2 nm)]$_5$ structures. (c) Distribution of the lattice parameters in the Co(0.8) and Co(1.6) superlattices. (d) Average strains in the bottom Pd/Co and top Co/Pd interfaces, as functions of the Co thickness; a_{Co0} is the bulk lattice parameter of fcc-Co.

from the beginning and is accompanied by the incorporation of misfit dislocations [35]. The strains in Co gradually relax but the degree of strains in the top Co atomic layers depends on the thickness of the Co that has already been grown. The thickness dependencies of the lattice parameters of the first three material layers, except for the Cu buffer layer in the $[Co(d_{Co})/Pd(2\,nm)]_5$ samples, are shown in Fig. 1(b). The parts of the curves where the lattice parameter decreases correspond to the Co growth. The lattice parameter restores to the Pd bulk value after the deposition of a Pd layer on top of a Co layer, if the thickness of the Co layer is 1.6 nm or less. If the first Co layer is thicker, then 2 nm of deposited Pd is not enough to restore the lattice parameter to the Pd bulk value, like it is in the case of the Co(2.4) superlattice in Fig. 1(b). Strains in the bottom Pd/Co interfaces of the second and upper Co layers decrease and begin to depend on the Co thickness, if it is thicker than 1.6 nm. We focused on the Co thickness interval less than 1.6 nm because the effective PMA is positive in this thickness interval. Distribution of the strains in all the layers in the Co(0.8) and Co(1.6) superlattices is indicated in Fig. 1(c). Since there is no explicit dependence of the lattice parameters of the interface layers on the layer number and standard deviation is small, we use average values of strains for the interface layers of a given superlattice independently of the number of a layer. The dependencies of the average strains in the bottom Pd/Co and top Co/Pd interfaces on the Co thickness are shown in Fig. 1(d). Asymmetry of strains between the bottom and top interface Co layers increases with increasing Co thickness.

It should be noted that we did not detect any meaningful differences in the roughness on the top of the $[Co(d_{Co})/Pd(2\,nm)]_5$ structures in the Co thickness interval of 0.6–1.6 nm. This may be related to the fact that Co tends to smooth the surface of the underlying Pd layer in the initial stages of the growth [36]. Hence, if the thickness of the Co layers is not quite large then the growth of Co on Pd does not lead to an increase in the roughness.

B. Magnetic properties and magnetization reversal

Magnetization reversal processes in the $[Co(d_{Co})/Pd(2\,nm)]_5$ multilayers strongly depend on the Co thickness. The OOP and IP hysteresis loops of the samples with a d_{Co} less than 1.6 nm are outlined in Figs. 2(a) and 2(b), respectively. The PMA decreases with an increase of the Co thickness, hence saturation fields in the IP hysteresis loops decrease. An increase in the Co thickness also leads to an increase of the magnetostatic energy of the system. These two factors result in the self-demagnetization of superlattices with thick Co layers. Magnetization reversal processes in the OOP directed magnetic fields change with increasing Co thickness. At low Co thickness ($d_{Co} < 0.6\,nm$), when the energy of PMA is very large, the hysteresis loops are rectangular and magnetization reversal occurs by the switching of the magnetization in the entire sample. An increase in d_{Co} leads to the emergence of "tails" in the OOP hysteresis loops in the regions of loops near saturation. These "tails" are related to the existence of domains which are
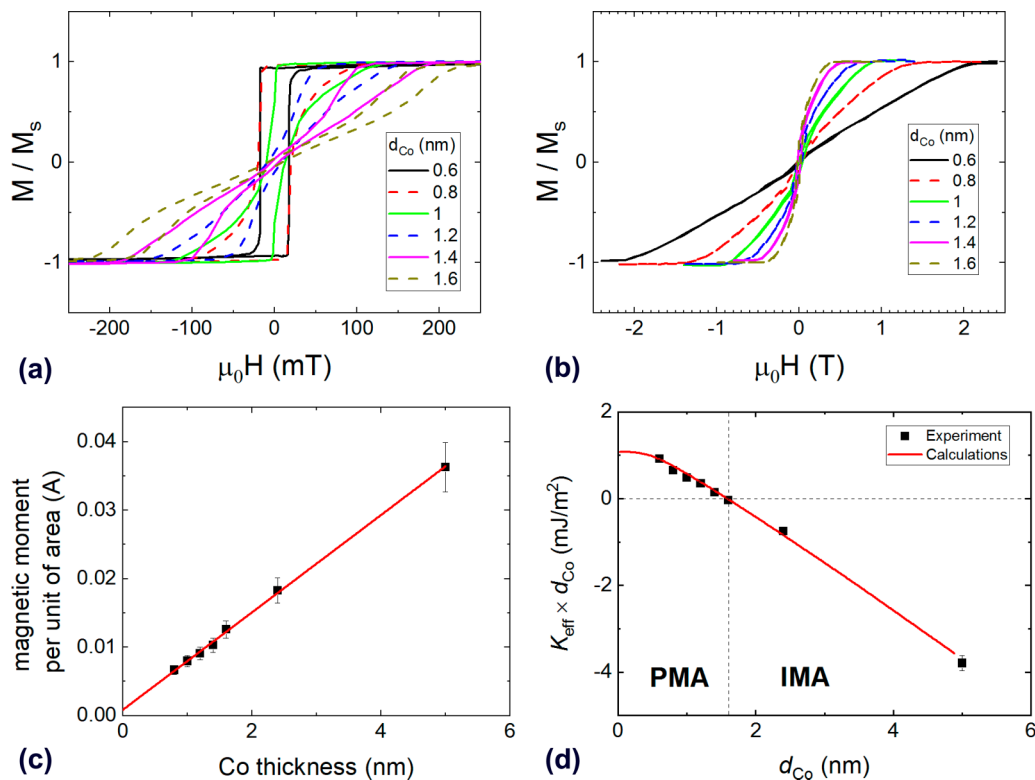
FIG. 2. (a) OOP and (b) IP hysteresis loops of crystalline $[Co(d_{Co})/Pd(2\,nm)]_5$ superlattices. The dependencies of (c) magnetic moment per unit of area, and (d) $K_{eff} \times d_{Co}$ on the Co thickness in the $[Co(d_{Co})/Pd(2\,nm)]_5$ superlattices.

quite stable in large magnetic fields and needed additional energy to be removed. These "tails" extend with increasing Co thickness ($d_{Co} = 0.6$–0.8 nm), however, normalized remanent magnetization still remains equal to unity. This particular thickness interval is interesting for practical applications because isolated domains stabilized in large negative magnetic fields remain almost unchanged after switching off the magnetic field. Further increases in the Co thickness make it possible to nucleate negatively magnetized domains, even in positive magnetic fields. Nucleated domains develop into a labyrinth domain structure in the remanent state. Negatively magnetized domains grow in size in negative magnetic fields, the labyrinth structure transforms into isolated stripe domains, then into bubble domains in the fields near negative saturation ($d_{Co} = 1$–1.6 nm). In this Co thickness interval the isolated magnetic domains develop to the labyrinth state in the remanent state, which is not favorable for racetrack memory devices, however, could be used to stabilize skyrmion lattices [37]. A more detailed description of the magnetization reversal processes of self-demagnetizing superlattices may be found in the paper of Davies *et al.* [38].

The dependence of the magnetic moment, normalized to the unity of an area, on the Co thickness measured in the $[Co(d_{Co})/Pd(2\,nm)]_5$ multilayers is shown in Fig. 2(c). It is well known that Pd interface layers are magnetically polarized in the vicinity of the Co layers [39]. Therefore, the net magnetic moment per unity of an area may be described as

$$\frac{m}{S} = 5M_{s,Co}d_{Co} + 10M_{s,Pd}d_{Pdpol}, \tag{1}$$

where m is a magnetic moment of the sample, S is an area of the film, $M_{s,Co}$, and $M_{s,Pd}$ are the saturation magnetizations of Co and polarized Pd, respectively; d_{Co}, and $d_{Pd\,pol}$ are the thicknesses of the deposited Co layers and the polarized interface Pd layers, respectively. The formula takes into account five Co layers and ten polarized Pd interface layers. Interception of the linear fitting of $m(t_{Co})/S$ dependence with the y axis gives a positive sum magnetic moment per unit area, $10M_{s,Pd}d_{Pd\,pol} = 7.5\times10^{-4}$ A, induced in all the Pd interface layers. Using the value of the saturation magnetization of Pd, $M_{s,Pd} = 0.31\times10^6$ A/m [40], the effective thickness of each of the polarized Pd interface layers is calculated as $d_{Pd\,pol} = 0.24$ nm, which agrees well with the result from our previous paper, 0.2 nm. The latter value is used in this paper. The slope of the $m(d_{Co})/S$ dependence in the $[Co(d_{Co})/Pd(2\,nm)]_5$ multilayers gives a value of saturation magnetization of $M_{s\,Co} = 1.43\times10^6$ A/m, which is close to the bulk value for Co. If one neglects the Pd polarized layers with low magnetization and assumes that all the magnetic material is concentrated in the Co layer, then the value of the saturation magnetization in the $[Co(d_{Co})/Pd(2\,nm)]_5$ superlattices is a function of the Co thickness:

$$M_s = \frac{M_{s,Co}d_{Co} + 2M_{s,Pd}d_{Pdpol}}{d_{Co}}. \tag{2}$$

These values of saturation magnetization were used in the calculation of the effective energy of PMA, K_{eff}. All the magnetic parameters are listed in Table I. The dependence of the $K_{eff}\times d_{Co}(d_{Co})$ is outlined in Fig. 2(d). Using the approach

TABLE I. Parameters of the epitaxial $[Co(d_{Co})/Pd(2\,nm)]_5$ superlattices.

d_{Co}	A	M_s	$\mu_0 H_{eff}$	K_{eff}	λ_{OOP}	λ_{IP}
(nm)	(pJ/m)	(kA/m^3)	(T)	MJ/m^3		(nm)
0.6	25	1626	1.89	1.5		
0.8		1575	1	0.79	820 ± 100	600 ± 50
1		1544	0.63	0.49	500 ± 40	335 ± 25
1.2		1523	0.39	0.29	248 ± 14	205 ± 10
1.4		1508	0.14	0.1	176 ± 8	141 ± 5
1.6		1497	−0.03	−0.02	150 ± 7	128 ± 3

proposed in our previous paper [36], we calculated the magnetoelastic and interface contributions to the surface energy of PMA in this system. Fitting the experimental data gives the interface magnetic anisotropy contribution $K_s = 1.1$ mJ/m^2 and magnetoelastic surface and volume contribution, $K_{s,\,MEA} = 0.81$ mJ/m^2 and $K_{v,\,MEA} = 0.16$ MJ/m^3, respectively. These values agree well with our results reported for single-layered $Pd(2.25\,nm)/Co(d_{Co})/Pd(2.25\,nm)$ films.

C. MFM measurements of the demagnetized domain structures

The period of the magnetic structures was determined by the averaging of 20–30 random distances between the centers of adjacent labyrinth domains on the experimental MFM image. The periodicity and anisotropy of the demagnetized labyrinth domain structure depend on the direction of an alternating demagnetizing field with a decreasing amplitude. If the magnetic field is oriented OOP, then the magnetic structure is isotropic. If the magnetic field is oriented IP, then magnetic stripes orient towards the field axis and the period is less than in the previous case. The OOP and IP demagnetized domain structures of $[Co(d_{Co})/Pd(2\,nm)]_5$ superlattices are shown in Figs. 3(a) and 3(b), respectively.

Regular domain patterns are observed when the Co thickness in the $[Co(d_{Co})/Pd(2\,nm)]_5$ superlattices is 1 nm and larger. The size of the stripe domains decreases with an increase of the Co thickness (Fig. 4). This phenomenon may be explained solely by the decreasing energy of PMA and the increasing magnetostatic energy of the system. Similar domain structures were observed in systems in which the DMI was supposed to be absent [26]. However, an addition of DMI in such systems lowers the energy of DWs [23] and hence leads to a decrease of domain sizes when compared with the case when the energy of effective DMI is zero.

D. Micromagnetic simulations

Micromagnetic simulations were carried out to estimate the energy of effective DMI in this system. Experimentally measured periodicities of the labyrinth domains are compared with periodicities of simulated magnetic structures with different effective DMI energies. Since the period of experimental domain structures depends on the direction of the demagnetizing field, two effective energies of DMI may be obtained: the first one if the simulated structures are compared with IP demagnetized images, and the second one if the simulated structures are compared with OOP demagnetized images. They will be referred to in the text as IP and OOP
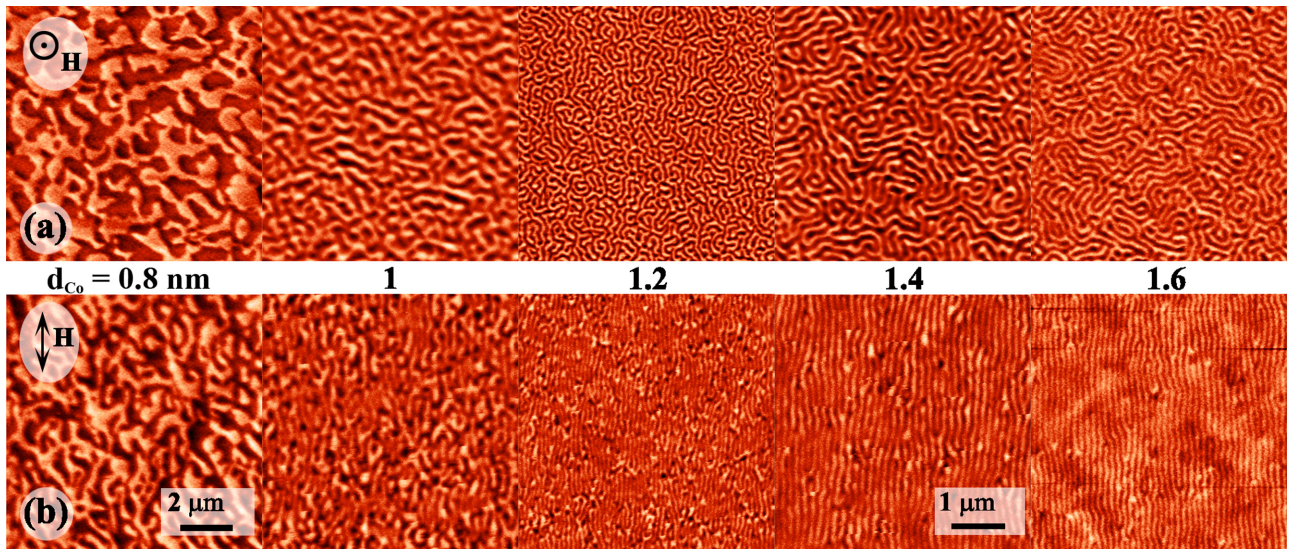
FIG. 3. MFM images of (a) OOP and (b) IP demagnetized domain structures of the $[Co(d_{Co})/Pd(2\,nm)]_5$ superlattices. Note that scale is halved reduced in the case of $d_{Co} = 1.4$ and 1.6 nm.

effective DMI energies ($D_{eff\,IP}$ and $D_{eff\,OOP}$), respectively. In micromagnetic simulations, we used a monodomain magnetic structure with two bubble domains as an initial state. The diameter of the bubbles was 100 nm [500 nm in the case of Co(0.8) samples]. The magnetic configuration was calculated in the remanent state by the evolution of isolated bubbles into the labyrinth domain state. In this case, the simulated magnetic structures are isotropic and match the OOP demagnetized experimental images well [Fig. 5(a)]. Therefore, it is natural to compare the OOP demagnetized structures with the simulated ones in the present case. In most of the papers a random initial state is used for the micromagnetic modeling of the labyrinth domain structures [7,23,30]. Relaxation of the random state in the zero magnetic field leads to the presence of domains with wide spread in width and a large number of skyrmions in relaxed states, which does not coincide with the experimental images [Fig. 5(b)]. A measurement of the period of labyrinth domains after the relaxation of the random mag-

netic state is possible only using a 2D fast Fourier transform (FFT) which gives reliable results only in the case of relatively large magnetic images. Labyrinth domain states relaxed from bubbles demonstrate uniform domain width and require less magnetic area in the simulations for the precise analysis.

We do not focus on the sign of the evaluated effective DMI energies, because the periodicities of the labyrinth domain structures obtained by micromagnetic modeling do not depend on the sign of D_{eff}. Based on the behavior of the domains under the influence of IP and OOP magnetic fields [15,16] we may conclude that the DMI induces predominantly right-handed chirality in the Néel DWs in the $[Co(0.6\,nm)/Pd(2\,nm)]_5$ superlattices. If we suppose that chirality does not change with increasing Co thickness in the $[Co(d_{Co})/Pd(2\,nm)]_5$ superlattices and use the DMI energy expression as in [34], a *negative* sign of the effective energies derived in the $[Co(d_{Co})/Pd(2\,nm)]_5$ superlattices should be considered.

The dependencies of the periods of simulated domain structures on the effective energy of the DMI for $d_{Co} = 0.8$, 1, 1.2, 1.4, and 1.6 nm in the $[Co(d_{Co})/Pd(2\,nm)]_5$ superlattices are shown in Figs. 5(c)–5(g), respectively. A comparison of the results obtained using the accurate and single z-cell effective models is also shown. The results obtained by singe z-cell and N-z-cell models are quite similar in the whole range of considered DMI energies. We found an excellent coincidence between the results of micromagnetic simulations and curves calculated by means of 2D [23] and 3D [24] analytical models which corroborates the reliability of the obtained results. The periods of labyrinth structures obtained by effective simulations (2D model) are sufficiently larger than periods obtained by means of accurate simulations (3D model) if the effective DMI constant is less than some critical value which depends on the Co thickness. This fact may be explained by the growing influence of magnetostatic energy in the case of thicker Co films. Effective models do not correctly take into account the magnetostatic interaction between the layers. Dipolar interaction may strongly influence both the size of the domains and
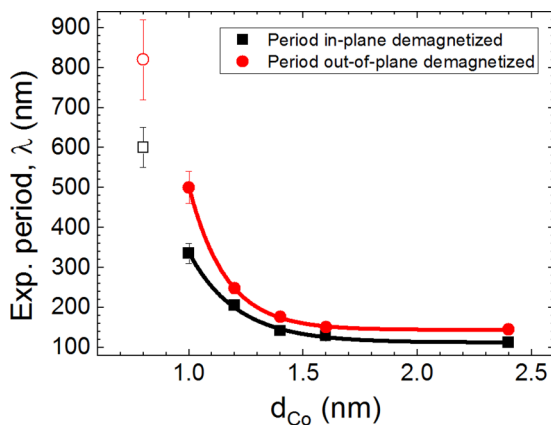

FIG. 4. Periods of the IP and OOP demagnetized stripe domain structures as functions of the Co thickness in the $[Co(d_{Co})/Pd(2\,nm)]_5$ superlattices [open symbols denote periods of irregular domain patterns of Co(0.8) samples].
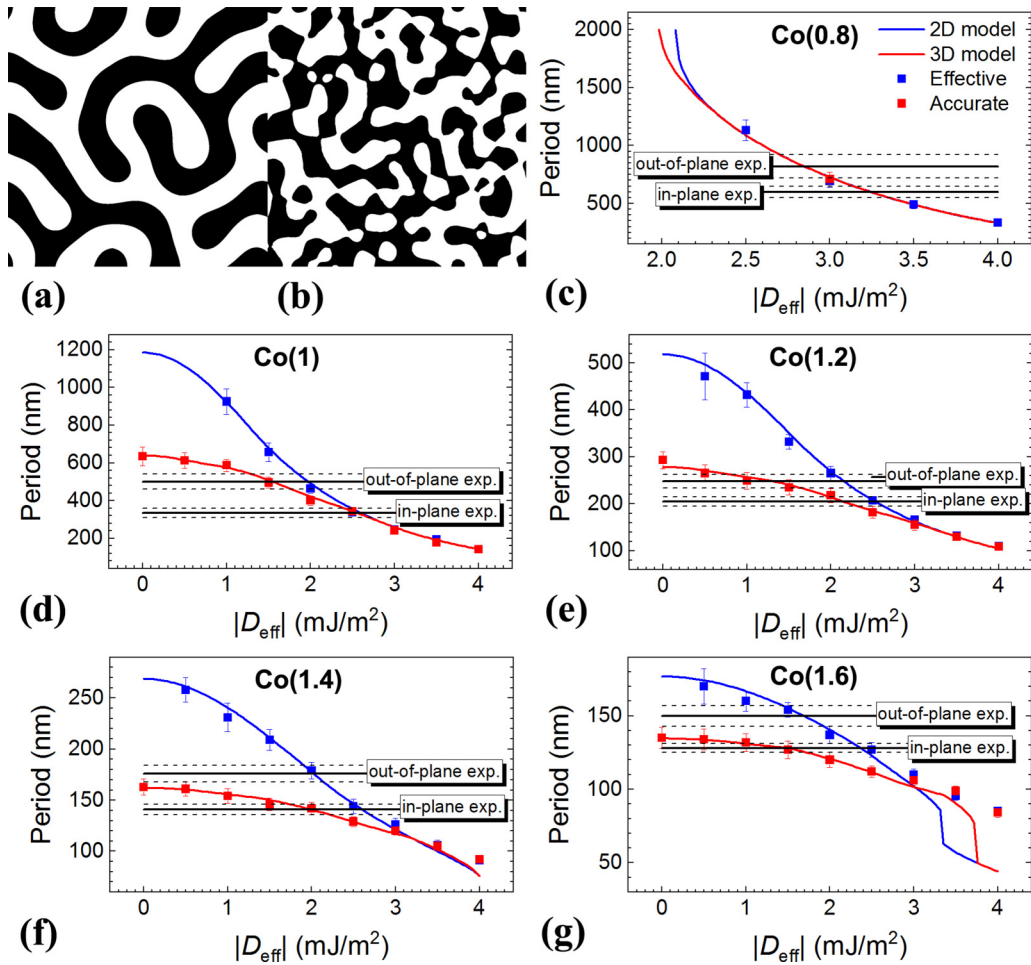
FIG. 5. Simulated magnetic structures of the Co(1) superlattice with $D_{eff} = 2\,mJ/m^2$ using (a) two bubbles, (b) random magnetization in the initial state. Comparison of the simulated periods of labyrinth domain structures with the experimentally obtained ones for the $[Co(d_{Co})/Pd(2\,nm)]_5$ superlattices with d_{Co} equal to (c) 0.8, (d) 1, (e), 1.2, (f) 1.4, and (g) 1.6 nm. Blue and red squares denote micromagnetic simulation results using effective and accurate models, respectively. Blue and red solid lines are calculated analytically using 2D [23] and 3D [24] models, respectively.

internal DWs structure. It was shown that dipolar interaction leads to hybrid chiral DWs with a Bloch-like structure in the center, even in the systems with nonzero DMI [24–26]. When DMI becomes stronger, the Bloch regions are pushed out to the surface of the films and the DWs become homochiral. The domain structure of the homochiral DWs becomes uniform throughout all the layers of the structure. Therefore, the results of the effective and accurate modeling converge to a single curve at large DMI energies. Based on the aforementioned results we claim that the accurate model has to be used in the micromagnetic modeling of the systems with the relation of the thicknesses of NM and FM layers less than 2.5, or a careful comparison of the results obtained by effective and accurate models needs to be carried out. The IP and OOP effective DMI energies of the samples with $d_{Co} = 0.8$–1.6 nm, using the results from the micromagnetic simulations based on the accurate model, are listed in Table II.

E. Discussion

A net surface DMI energy D_s, may be derived by means of the value of effective DMI energy using the following formula:

$$D_S = D_{eff} d_{Co}. \tag{3}$$

The effective and surface DMI energies estimated by the comparison of the periodicities of magnetic structures obtained by accurate modeling and MFM are outlined in Figs. 6(a) and 6(b), respectively. The error values are determined using the uttermost points of the intersections of the analytically calculated solid curves with experimental periodicity bars in Fig. 5. In a simple phenomenological model, taking into account that DMI is of an interface origin in this system, the surface DMI energy is considered to be a constant. Thus, the dependencies of the IP effective and surface DMI energies on the Co thickness are more reasonable than for the respective OOP energies. The $|D_{S\,OOP}|$ values strongly decrease with increasing of the Co thickness, which could not be explained by the phenomenological model. The only explanation of this may be that the net surface DMI energy is not a constant but it depends on the Co thickness. Let us suppose that nonzero net DMI in this system is proportional to the asymmetry of the strains between the bottom Pd/Co and top Co/Pd interfaces. While the strains in the bottom Pd/Co

TABLE II. Effective DMI energies obtained in this paper and in other systems with the same Co thickness.

d_{Co}	$|D_{eff\,IP}|$	$|D_{eff\,OOP}|$	System	$|D_{eff}|$
(nm)	(mJ/m^2)			(mJ/m^2)
0.8	1.67 ± 0.4	1.15 ± 0.4	[Co/Ir(1 nm)/Pt(1 nm)]$_5$ [26]	1.64
1	2.55 ± 0.2	1.5 ± 0.25	Pt(2 nm)/Co/IrMn(2.4) [43]	1.22
1.2	2.1 ± 0.2	1.2 ± 0.4	Pt/Co/AlO$_x$ [4]	1.15
1.4	2 ± 0.2		Pt/Co/AlO$_x$ [44]	$\cong 0.46$
1.6	1.4 ± 0.35		Pt/Co/AlO$_x$ [4]	0.7

interfaces are the same for all of the samples, the top Co/Pd interfaces undergo different strains. The difference between the strains in the bottom Pd/Co and top Co/Pd interfaces increases with increasing Co thickness. Therefore, the net surface DMI should increase with an increase of the Co thickness, which is not observed in both the cases of IP and especially OOP DMI energies.

To increase the reliability of the results we decided to compare the results of our previous investigation [33] with the current results. In the previous paper, we investigated the dependence of the effective DMI energy on the number of Co/Pd bilayers $N = 1$–20 in the [Co(0.8 nm)/Pd(2 nm)]$_N$ superlattices using the single z-cell effective model in micromagnetic simulations. The present series of the samples intersects with the N series at $d_{Co} = 0.8$ nm ($N5$ sample in the N series). Hence, the effective DMI energies of Co(0.8) and $N5$ samples determined by the domain-period method $|D_{eff\,OOP}| = 2.9 \pm 0.15$ and $|D_{eff\,IP}| = 3.2 \pm 0.1$ mJ/m^2 must be the same. We reran the micromagnetic simulations of the labyrinth domain structures for the $N10$ and $N20$ samples using the accurate model instead of the effective model. Also, we used the latest value of $D_{eff} = 0.6 \pm 0.1$ mJ/m^2 for the $N1$ samples. The values of effective DMI energies determined by the domain-period method for Co(0.8) samples does not fit to the $D_{eff}(N)$ dependencies completely (Fig. 7). A sudden maximum of effective DMI in the $N5$ samples is improbable. Moreover, we simulated OOP hysteresis loops for $N5$ samples with different DMI constants (see the Appendix for details) and found the best coincidence with the experimental OOP loops if D_{eff} lies in the interval from 0.4 to 1.6 mJ/m^2

which is sufficiently less than the DMI energies determined by the periodicity analysis. Then we fitted the three point plots $D_{eff}(N = 1, 10, 20)$ using the exponential function $y = y_0 + Ae^{R_0 x}$, and found the values of $D_{eff\,IP} = 1.67 \pm 0.5$ mJ/m^2 and $D_{eff\,OOP} = 1.14 \pm 0.5$ mJ/m^2 for $N5$ or Co(0.8) samples, which agree quite well with the results of the hysteresis loops analysis.

Substitution of the effective DMI energies obtained for N series of samples to the $D_{eff}(d_{Co})$ dependencies in Fig. 6(a) leads to a decrease of effective DMI in the Co(0.8) superlattices, while effective DMI of the interface origin should increase with decreasing thickness of the magnetic layer. However, a decrease of the surface DMI energy in the low FM layer thickness regime is frequently observed in various systems [4,41,42]. This may be explained by structural inhomogeneity or by the degradation of the top FM/NM interface.

Magnetic hysteresis loops for the samples of the Co series are shown in the Appendix. The comparison of the simulated and experimental hysteresis loops allows us to estimate DMI energies, however, errors of determined values are large. The results are also indicated in Fig. 6. It is worthwhile to note that DMI energies obtained by the hysteresis loops analysis $D_{eff\,loops}$ and $D_{S\,loops}$ match better with the OOP DMI energies.

One may notice that the $\lambda(D_{eff})$ dependencies analytically calculated for the Co(1.4) and Co(1.6) samples do not intersect with the bands of experimentally obtained OOP demagnetized periods in Figs. 5(f) and 5(g). OOP DMI energies at $d_{Co} = 1.4$ and 1.6 nm in Fig. 6 are set to zero values but strictly speaking the method does not work at these points, thus these points are marked as red crosses. The $\lambda(D_{eff})$
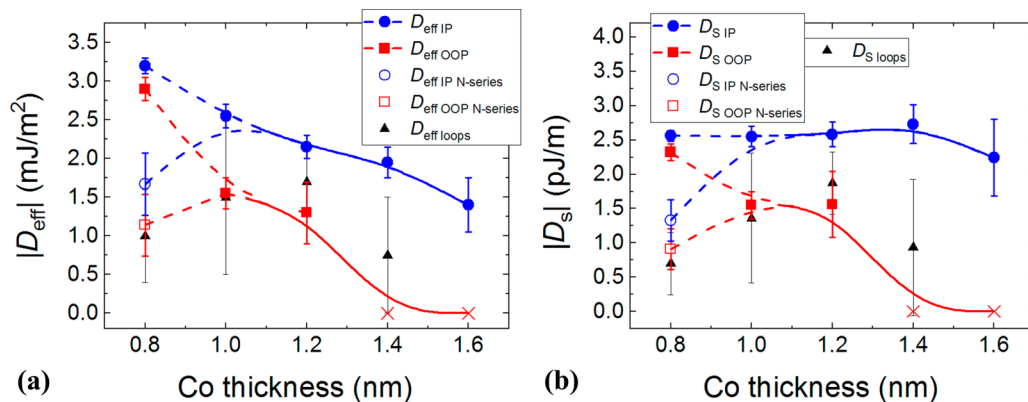

FIG. 6. The absolute values of (a) effective, and (b) surface DMI energies depending on the Co thickness in the crystalline [Co(d_{Co})/Pd(2 nm)]$_5$ superlattices. Solid lines are B-spline interpolation curves. Open points are determined based on the results of the previous paper [33]. Red crosses indicate the points where the domain-period method doesn't work.
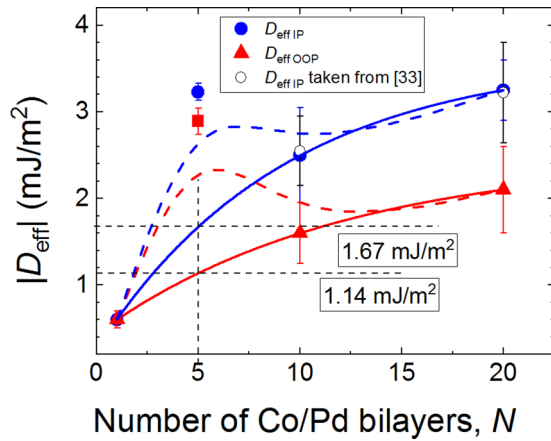
FIG. 7. The absolute values of effective DMI energies depending on the number of Co/Pd bilayers in the crystalline $[Co(0.8\,nm)/Pd(2\,nm)]_N$ superlattices. Solid lines denote exponential fitting of the obtained $D_{eff}(N = 1, 10, 20)$ dependencies. Dashed lines are the B-spline interpolated curves based on all points. Points on the graph are obtained by means of the domain-period method except the $N1$ point.

dependencies must at least reach the experimental range of values at the point of $D_{eff} = 0$, otherwise micromagnetic parameters must be reconsidered. Another point that needs discussing is the absolute values of obtained DMI energies. IP effective DMI energies in the investigated superlattices are rather large when compared with reported data for other systems with the same thickness of Co layers, as indicated in Table II. The values for the IP effective DMI energies at large Co thicknesses near the spin reorientation transition of the magnetization to the plane of the structures are especially doubtful. The values for the OOP effective DMI energies seem more reasonable, taking into account that the investigated system is symmetric by the composition. However, the problem of determination of the OOP effective DMI energies in the Co(1.4) and Co(1.6) samples requires solution.

Two parameters are quite flexible in the domain-period method: the exchange constant and the saturation magnetization. Values of the exchange constant used for the investigation of polycrystalline Co belong to the interval 10–16 pJ/m [6,29,30], while the experimentally measured values of the exchange constant of crystalline Co are 25–36 pJ/m [40,43,44]. A good compromise would be to use the exchange constant in the range 20–30 pJ/m. The saturation magnetization was determined including Pd polarized layers in the magnetic layers. In this case, the saturation magnetization is variable and depends on the Co thickness. However, it is arguable, because the saturation magnetization of Pd is nearly 4.5 times less than the saturation magnetization of Co. Therefore, it is quite reasonable to neglect magnetically polarized Pd layers and use the bulk value of the saturation magnetization of Co, $M_s = 1420\,kA/m^3$. In this case, the energy of the PMA must be recalculated as well. Taking into account the excellent coincidence of the results of accurate micromagnetic simulations and analytical calculations by the 3D model [24] it was decided to use analytical calculations due to significantly speeding up the research.

The IP effective and surface DMI energies analytically calculated by the 3D model for different exchange constants and bulk value of the saturation magnetization are shown in Figs. 8(a) and 8(b), respectively. Dependencies $|D_{eff\,IP}(d_{Co})|$ and $|D_{S\,IP}(d_{Co})|$ calculated for $A = 25\,pJ/m$ and variable M_s are added for comparison. We did not consider $d_{Co} = 0.8\,nm$ due to controversial results from Co and N series of samples. Using bulk Co magnetization and fixed exchange constant $A = 25\,pJ/m$ in the analytical model results in increasing the numerical values of the $|D_{eff\,IP}(d_{Co})|$ and $|D_{S\,IP}(d_{Co})|$ curves compared to calculations obtained for variable M_s. Slope of the curves and numerical values may be also adjusted by variation of the exchange constant. Therefore, we find that results calculated for $A = 25\,pJ/m$ and variable M_s are nearly equal to the results calculated for $A = 23\,pJ/m$ and $M_s = 1420\,kA/m^3$. Decreasing the exchange constant to the values of 20 pJ/m leads to a sudden drop of the $D_{S\,IP}$ in the Co(1.6) superlattices to zero which is highly improbable. Suppose that different strains in the top Co/Pd interface are the origin of the Co thickness dependence of the surface DMI energy. Strains in the top Co/Pd interface decrease linearly with increasing the Co thickness beginning from 1 nm. Therefore, it is reasonable to expect the smooth Co thickness dependence of the surface DMI energy in the interval of Co thicknesses from 1 to 1.6 nm. The behavior of the $|D_{eff\,IP}(d_{Co})|$ and $|D_{S\,IP}(d_{Co})|$ curves depending on the value of the exchange energy is similar, both in the case of the variable M_s and in the case of the constant M_s [Figs. 8(c) and 8(d)]. Using exchange constants larger than 25 pJ/m leads to larger $D_{eff\,IP}$ and $D_{S\,IP}$ values which do not match literature data. Using lower exchange constants lead to a drop of the $D_{S\,IP}$ in the Co(1.6) superlattices as in the case with $M_s = 1420\,kA/m^3$.

The OOP effective and surface DMI energies calculated for constant and variable M_s and different exchange constants are indicated in Figs. 8(e)–8(h). More or less adequate behavior of the $D_{S\,OOP}$ without sudden drops but still largely dependent on the Co thickness is obtained for $A = 30\,pJ/m$ and $M_s = 1420\,kA/m^3$. In other cases, surface DMI constant decreases to zero in the superlattices with large Co thickness.

Analysis of the calculated results obtained for different values of the exchange constant and the saturation magnetization indicate that the Co thickness dependencies of the IP effective and surface DMI energies in the $[Co(1–1.6\,nm)/Pd(2\,nm)]_5$ structures are more acceptable and stable to small deviations of micromagnetic parameters. The OOP effective and surface DMI energies are reasonable only for $M_s = 1420\,kA/m^3$ and the limit value of $A = 30\,pJ/m$.

The ordering of the experimental demagnetized images depends on the direction of the demagnetizing field. It is natural to expect lower periodicity in the ordered stripe domain state because with the same total length of the domain walls, as in the disordered labyrinth magnetic pattern, density of the ordered domains will be larger. Therefore, one might expect different periods of the equilibrium ordered stripe and disordered labyrinth micromagnetic patterns. We checked this assumption by calculating the total energy density of ten ordered stripes depending on the period size with different DMI energies for Co(1.4) sample using micromagnetic parameters $A = 25\,pJ/m$ and $M_s = 1508\,kA/m^3$. The periodicity of the domains was changed by choosing the appropriate size of
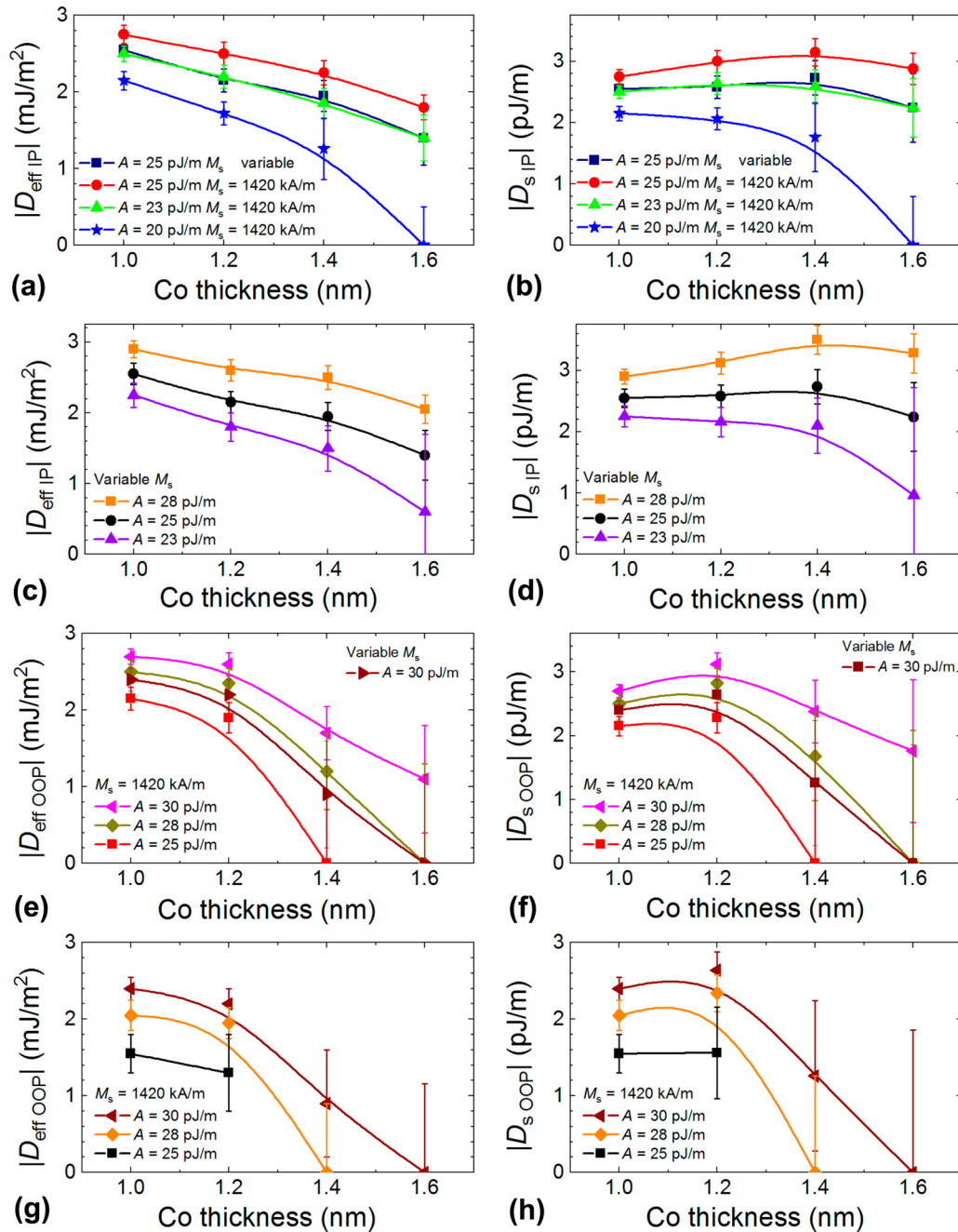
FIG. 8. The dependencies of $|D_{eff\,IP}(d_{Co})|$ and $|D_{S\,IP}(d_{Co})|$ calculated for (a), (b) constant M_s, (c), (d) variable M_s, respectively. The dependencies of $|D_{eff\,OOP}(d_{Co})|$ and $|D_{S\,OOP}(d_{Co})|$ calculated for (e), (f) constant M_s, (g), (h) variable M_s, respectively. The exchange constant A is varied in each case. Points denote results of analytical calculations by 3D model [24]. Solid lines are *B*-spline interpolations.

a simulation area like it was carried out in [29]. A ground state with a certain period for given magnetic parameters was determined in the point of minimal total energy density [see the inset in Fig. 9(a)]. The striking result is a coincidence of $\lambda(D_{eff})$ dependencies obtained by micromagnetic modeling of labyrinth (developed from two bubbles) and ordered (artificially defined) stripe domain structures [Fig. 9(a)]. Similar result was also obtained by Lemesh *et al.* while testing a 2D analytical model via micromagnetic simulations of ordered stripe and labyrinth domain configurations obtained after relaxation from a random magnetic state [23]. It is worthwhile to note that equilibrium periodicities calculated

as a result of simulations from the random initial magnetic state are slightly lower than periodicities of ordered magnetic states. The periods of regular labyrinth domain structures calculated for Co(1.4) superlattices defined by the FFT are slightly larger than periods defined by statistical profile analysis.

Total-energy densities of equilibrium states of Co(1.4) superlattices obtained from different initial magnetic configurations are outlined in Fig. 9(b). The ordered stripe magnetic state has the lowest total-energy density over the entire considered DMI energy range. While the total-energy density of the isotropic labyrinth state is larger than the total-energy
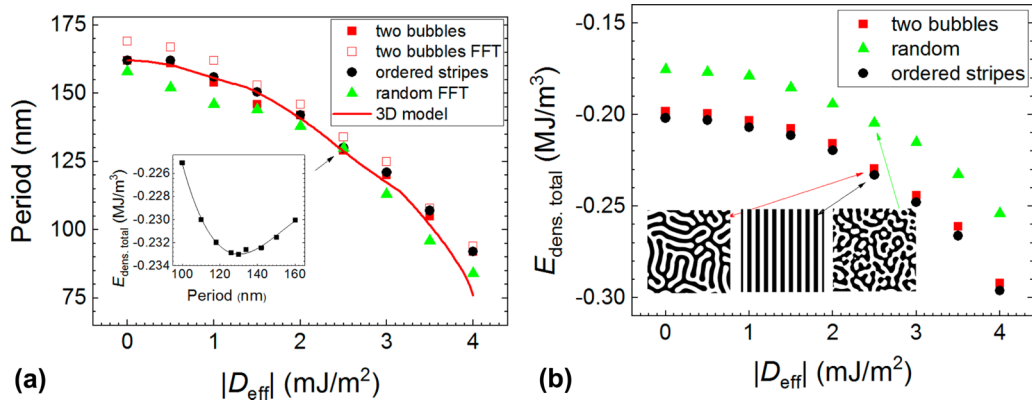
FIG. 9. (a) Periods of magnetic structures of Co(1.4) superlattices simulated from different initial configurations and determined by FFT or statistical profile analysis. The dependence of the total-energy density of the ordered magnetic state on the period for $|D| = 2.5\,\mathrm{mJ/m^2}$ is indicated in the inset. (b) Total-energy densities as functions of the absolute values of effective DMI energies calculated from different initial magnetic configurations. $2\,\mu\mathrm{m} \times 2\,\mu\mathrm{m}$ equilibrium magnetic configurations calculated for $|D| = 2.5\,\mathrm{mJ/m^2}$ are shown in the inset.

density of the ordered stripe state by nearly $4\,\mathrm{kJ/m^3}$, the total-energy density of the magnetic state minimized from a random magnetic structure is larger than the total-energy density of the ordered stripe on the average by $30\,\mathrm{kJ/m^3}$. Therefore, magnetic configurations obtained after the relaxation of the random magnetic states are far from ground states in this case. Nevertheless, the obtained periodicity does not depend significantly on the initial magnetic configuration [see the inset in Fig. 9(b)].

In spite of the micromagnetic modeling results, the periods of the ordered IP and labyrinth OOP demagnetized structures differ significantly. Therefore, it is necessary to establish which state of the two above is closer to the ground state. The difference in periods may be related with a pinning of domain walls on defects and different evolution of magnetic structures during the magnetization reversal in differently oriented magnetic fields. Since the previously considered magnetic states were simulated without any magnetic fields we calculated magnetic structures of Co(1.4) superlattices in magnetic fields of IP and OOP orientations with a decaying magnitude from saturation field to zero. Two circular magnetic defects with a diameter of 100 nm and fixed opposite OOP magnetization were included in the simulation. The following micromagnetic parameters were used: $A = 25\,\mathrm{pJ/m}$, $M_s = 1508\,\mathrm{kA/m^3}$, $D_{\mathrm{eff}} = 0.5\,\mathrm{mJ/m^2}$. A remanent magnetic state developed after the gradual demagnetization in the OOP magnetic field demonstrated a period of 159 ± 6 nm, the same as in the magnetic patterns obtained after the relaxations of two bubbles in zero magnetic field. Changes in the magnetic structure of self-demagnetizing samples occurring with a decrease in the perpendicular magnetic field are well described in the literature [38] and corroborated by the results of our simulations. Bubbles or skyrmions nucleated in high magnetic fields grow into stripes, the density of which increases with decreasing magnetic field. Therefore, the periodicity of the isotropic labyrinth structure decreases with decreasing magnetic field. The period of experimental OOP demagnetized structures may be larger than the period in the ground state if a sample is not completely demagnetized due to pinning of the domain walls on defects. The OOP demagnetized experimen-

tal domain structures are isotropic with equal areas of dark and bright domains except in the Co(0.8) superlattice. Hence, we may conclude that defects have a minor effect on the period of the OOP demagnetized [Co(1–1.6 nm)/Pd(2 nm)]$_5$ structures.

The magnetic structure of Co(1.4) superlattices simulated in decaying IP magnetic fields from the magnetic saturation state demonstrated nucleation of ordered stripes with the period of 110 ± 2 nm in the magnetic field $\mu_0 H = 300$ mT. With decreasing the magnetic field, the density of stripes gradually increased by annihilation of isolated magnetic stripes and straightening of branched domains. The period of the stripe domain structure was equal to 153 ± 2 nm in zero magnetic field. This value is slightly lower than the period of the artificially defined stripes with minimal total-energy density. However, defects in the experimental structures may prevent annihilation of domain walls during the IP demagnetization procedure and lead to lower periodicities of IP demagnetized structures than in the ground state. Careful examination of the experimentally obtained IP demagnetized domain structures of [Co/Pd]$_5$ superlattices indicates the presence of a large number of defects such as branching, twisting, and breaking of the stripes. An ordering of the stripes and a decrease of the number of defects is observed with an increase in the Co thickness of [Co/Pd]$_5$ superlattices. A relative difference between the periods of OOP and IP demagnetized structures calculated by the formula $(\lambda_{\mathrm{OOP}} - \lambda_{\mathrm{IP}})/\lambda_{\mathrm{IP}}$ decreased from 0.49 to 0.17 with increasing Co thickness from 1 to 1.6 nm, which correlates with decreasing of the number of defects. Hence, it is reasonable to suggest that evolution of the stripe domain structure with a decrease of the IP magnetic field from the high dense state to the low dense state is more sensitive to the defects than development of the stripe domain structure from isolated stripes in OOP magnetic fields.

IV. CONCLUSIONS

The structural and magnetic properties of epitaxial [Co(d_{Co})/Pd(2 nm)]$_5$ superlattices were investigated with regard to their dependence on the Co thickness. The asymmetry
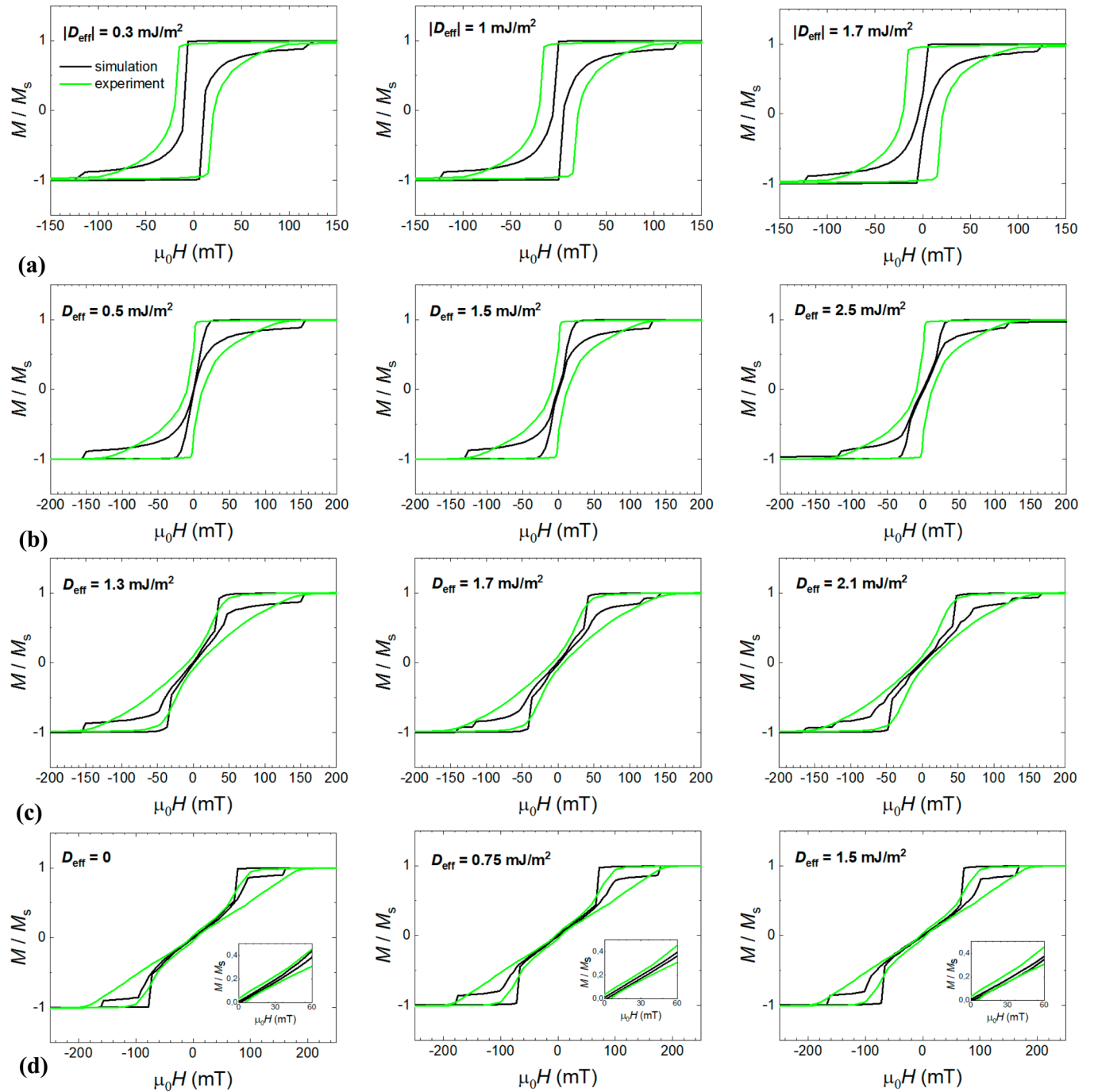
FIG. 10. Experimental and simulated with different values of the effective DMI energies OOP magnetic hysteresis loops of (a) Co(0.8) or N5, (b) Co(1), (c) Co(1.2), and (d) Co(1.4) superlattices.

of the strains between the lower Pd/Co and upper Co/Pd interfaces increases with an increase in the Co thickness. IP and OOP demagnetized structures were experimentally measured in epitaxial [Co(d_{Co})/Pd(2 nm)]$_5$ superlattices. The effective and surface energies of the DMI in this system were determined by the comparison of the periods of simulated domain structures and stripe domain structures, experimentally measured after the demagnetization of the samples in IP and OOP magnetic fields.

The results of the present work indicate that it is appropriate to use accurate micromagnetic simulations with all

the layers defined, or the 3D analytical model [24] for the systems with a relation of the thicknesses of NM and FM layers less than 2.5. Using a random magnetization as an initial magnetic state in micromagnetic simulations leads to labyrinth structures with higher total-energy densities and slightly lower periods than for the ground states. The method gives controversial results with the samples which do not self-demagnetize and demonstrate an $M_r/M_s = 1$ in the OOP hysteresis loops (Co 0.8 sample in this paper). The stripe domain structures of such samples after a forced demagnetization are irregular and the periods of these structures

could not be precisely determined by the analysis of 2D FFT spectra.

Analysis of the Co thickness dependencies of the DMI energies reveals that using experimentally obtained IP demagnetized structures rather than OOP demagnetized domain structures in the domain-period method gives more solid results. The dependencies of the IP effective and surface DMI energies on the Co thickness in the $[Co(d_{Co})/Pd(2\,nm)]_5$ superlattices are smoother and without unexpected abrupt changes, as compared to the dependencies of the OOP DMI energies. The values of the exchange constants used in the calculations of the IP DMI energies are more reasonable when compared to the exchange constants taken from the simulations of the OOP DMI energies.

The quantitative results obtained by the considered method strongly depend on the choice of the exchange constant. In the present work, relatively small deviations of the exchange constant, from 23 to 28 pJ/m, lead to a change in the qualitative behavior of the $D_{S\,IP}$ as a function of the Co thickness. The difference between IP and OOP DMI energies may be almost eliminated by an appropriate choice of the exchange constant value. We conclude that the domain-period method used with a fixed exchange constant may give qualitatively reliable results for quite different samples, such as samples with different stacking sequences of the layers or different heavy metal layers adjacent to the Co layers. However, a precise experimental determination of the exchange constant is needed for a correct definition of the behavior of DMI energies regarding their dependence on the thickness of the Co layers in the investigated structures.

Nevertheless, the results of the applied method indicated the presence of strong interfacial DMI in the $[Co(d_{Co})/Pd(2\,nm)]_5$ superlattices. The appropriate choice of Co thickness provides the opportunity to tune the energy of effective DMI and control the magnetic structures in the epitaxial $[Co(d_{Co})/Pd(2\,nm)]_5$ superlattices. Taking into account the opportunity of controlling the energy of effective DMI in this system by varying the number of Co/Pd bilayers it may be concluded that the epitaxial $[Co/Pd]_N$ multilayered structure is a system with flexible magnetic parameters, which is promising as a medium for skyrmion memory engineering.

APPENDIX: METHOD FOR THE ESTIMATION OF THE ENERGIES OF DZYALOSHINSKII-MORIYA INTERACTION BY ANALYSIS OF HYSTERESIS LOOPS

The approach for estimating the effective energy of DMI by comparing experimental and modeled hysteresis loops gives results with a large error. Therefore, such a method cannot be used as the main result, but may give complementary results. As the criteria of coincidence, we analyzed the tilting of the hysteresis loops in the near-zero magnetic fields and the values of the normalized remanent magnetization. Hysteresis loops simulated for the Co(0.8) superlattices are shown in Fig. 10(a). The coercive force of the experimental and simulated loops is different due to structural defects that are not taken into account in the simulations. The hysteresis loops simulated with $D_{eff} < 0.4$ and $>1.6\,mJ/m^2$ definitely do not fit with the experimental one. The simulated hysteresis loop with $D_{eff} = 0.3\,mJ/m^2$ is more rectangular than experimental one, and the normalized remanent magnetization of the hysteresis loop in the case of $D_{eff} = 1.7\,mJ/m^2$ is less than 1. However, the effective DMI energies that are in the fairly broad range of 0.4–$1.6\,mJ/m^2$ give identical hysteresis loops in the simulations, which fit the experimental ones quite well. Simulations for the Co(1) superlattices shown in Fig. 10(b) give effective DMI values of $D_{eff\,loops} = 1.5 \pm 1\,mJ/m^2$ with a large error. The most accurate values of the effective DMI energy are obtained in the Co(1.2) samples, $D_{eff\,loops} = 1.7 \pm 0.4\,mJ/m^2$, as shown in Fig. 10(c). However, hysteresis loops of the Co(1.4) [Fig. 10(d)] and especially Co(1.6) superlattices weakly depend on the effective DMI constant. Thus, we considered $D_{eff\,loops} = 0.75 \pm 0.75\,mJ/m^2$ for the Co(1.4) superlattices and excluded the hysteresis loops of the Co(1.6) samples from the consideration.

[1] I. Dzyaloshinsky, J. Phys. Chem. Solids **4**, 241 (1958).

[2] T. Moriya, Phys. Rev. **120**, 91 (1960).

[3] M. Belmeguenai, J. P. Adam, Y. Roussigne, S. Eimer, T. Devolder, J. V. Kim, S. M. Cherif, A. Stashkevich, and A. Thiaville, Phys. Rev. B **91**, 180405(R) (2015).

[4] J. Cho, N.-H. Kim, S. Lee, J.-S. Kim, R. Lavrijsen, A. Solignac, Y. Yin, D.-S. Han, N. J. J. van Hoof, H. J. M. Swagten, B. Koopmans, and C.-Y. You, Nat. Commun. **6**, 7635 (2015).

[5] H. Yang, A. Thiaville, S. Rohart, A. Fert, and M. Chshiev, Phys. Rev. Lett. **115**, 267210 (2015).

[6] C. Moreau-Luchaire, C. Moutafis, N. Reyren, J. Sampaio, C. A. F. Vaz, N. Van Horne, K. Bouzehouane, K. Garcia, C. Deranlot, P. Warnicke, P. Wohlhüter, J. M. George, M. Weigand, J. Raabe, V. Cros, and A. Fert, Nat. Nanotechnol. **11**, 444 (2016).

[7] A. Soumyanarayanan, M. Raju, A. L. G. Oyarce, A. K. C. Tan, M. Y. Im, A. P. Petrovic, P. Ho, K. H. Khoo, M. Tran, C. K. Gan, F. Ernult, and C. Panagopoulos, Nat. Mater. **16**, 898 (2017).

[8] S. Emori, U. Bauer, S. M. Ahn, E. Martinez, and G. S. Beach, Nat. Mater. **12**, 611 (2013).

[9] W. Jiang, P. Upadhyaya, W. Zhang, G. Yu, M. B. Jungfleisch, F. Y. Fradin, J. E. Pearson, Y. Tserkovnyak, K. L. Wang, O. Heinonen, S. G. E. te Velthuis, and A. Hoffmann, Science **349**, 283 (2015).

[10] S. Woo, K. Litzius, B. Krüger, M. Y. Im, L. Caretta, K. Richter, M. Mann, A. Krone, R. M. Reeve, M. Weigand, P. Agrawal, I. Lemesh, M.A. Mawass, P. Fischer, M. Kläui, and G. S. D. Beach, Nat. Mater. **15**, 501 (2016).

[11] A. Fert, V. Cros, and J. Sampaio, Nat. Nanotechnol. **8**, 152 (2013).

[12] S. Parkin and S. H. Yang, Nat. Nanotechnol. **10**, 195 (2015).

[13] S. Tacchi, R. E. Troncoso, M. Ahlberg, G. Gubbiotti, M. Madami, J. Akerman, and P. Landeros, Phys. Rev. Lett. **118**, 147201 (2017).

[14] M. A. Ordal, L. L. Long, R. J. Bell, S. E. Bell, R. R. Bell, R. W. Alexander, Jr., and C. A. Ward, Appl. Opt. **22**, 1099 (1983).

[15] S.-G. Je, D.-H. Kim, S.-C. Yoo, B.-C. Min, K.-J. Lee, and S.-B. Choe, Phys. Rev. B **88**, 214401 (2013).

[16] A. Hrabec, N. A. Porter, A. Wells, M. J. Benitez, G. Burnell, S. McVitie, D. McGrouther, T. A. Moore, and C. H. Marrows, Phys. Rev. B **90**, 020402 (2014).

[17] D.-H. Kim, D.-Y. Kim, S.-C. Yoo, B.-C. Min, and S.-B. Choe, Phys. Rev. B **99**, 134401 (2019).

[18] K. Shahbazi, J.-V. Kim, H. T. Nembach, J. M. Shaw, A. Bischof, M. D. Rossell, V. Jeudy, T. A. Moore, and C. H. Marrows, Phys. Rev. B **99**, 094409 (2019).

[19] M. Vaňatka, J. C. Rojas-Sánchez, J. Vogel, M. Bonfim, M. Belmeguenai, Y. Roussigné, A. Stashkevich, A. Thiaville, and S. Pizzini, J. Phys.: Condens. Matter **27**, 326002 (2015).

[20] K. S. Ryu, L. Thomas, S. H. Yang, and S. Parkin, Nat. Nanotechnol. **8**, 527 (2013).

[21] S. Kim, P. H. Jang, D. H. Kim, M. Ishibashi, T. Taniguchi, T. Moriyama, K. J. Kim, K. J. Lee, and T. Ono, Phys. Rev. B **95**, 220402(R) (2017).

[22] E. C. Corredor, S. Kuhrau, F. Kloodt-Twesten, R. Fromter, and H. P. Oepen, Phys. Rev. B **96**, 060410(R) (2017).

[23] I. Lemesh, F. Buttner, and G. S. D. Beach, Phys. Rev. B **95**, 174423 (2017).

[24] I. Lemesh and G. S. D. Beach, Phys. Rev. B **98**, 104402 (2018).

[25] W. Legrand, J. Y. Chauleau, D. Maccariello, N. Reyren, S. Collin, K. Bouzehouane, N. Jaouen, V. Cros, and A. Fert, Sci. Adv. **4**, eaat0415 (2018).

[26] S. A. Montoya, S. Couture, J. J. Chess, J. C. T. Lee, N. Kent, D. Henze, S. K. Sinha, M.-Y. Im, S. D. Kevan, P. Fischer, B. J. McMorran, V. Lomakin, S. Roy, and E. E. Fullerton, Phys. Rev. B **95**, 024415 (2017).

[27] O. Hellwig, A. Berger, J. B. Kortright, and E. E. Fullerton, J. Magn. Magn. Mater. **319**, 13 (2007).

[28] P. Agrawal, F. Buttner, I. Lemesh, S. Schlotter, and G. S. D. Beach, Phys. Rev. B **100**, 104430 (2019).

[29] M. Bacani, M. A. Marioni, J. Schwenk, and H. J. Hug, Sci. Rep. **9**, 3114 (2019).

[30] D. A. Dugato, J. Brandao, R. L. Seeger, F. Beron, J. C. Cezar, L. S. Dorneles, and T. J. A. Mori, Appl. Phys. Lett. **115**, 182408 (2019).

[31] S. Schlotter, P. Agrawal, and G. S. D. Beach, Appl. Phys. Lett. **113**, 092402 (2018).

[32] S. D. Pollard, J. A. Garlow, J. W. Yu, Z. Wang, Y. M. Zhu, and H. Yang, Nat. Commun. **8**, 14761 (2017).

[33] A. V. Davydenko, A. G. Kozlov, A. G. Kolesnikov, M. E. Stebliy, G. S. Suslin, Y. E. Vekovshinin, A. V. Sadovnikov, and S. A. Nikitov, Phys. Rev. B **99**, 014433 (2019).

[34] A. Vansteenkiste, J. Leliaert, M. Dvornik, M. Helsen, F. Garcia-Sanchez, and B. Van Waeyenberge, AIP Adv. **4**, 107133 (2014).

[35] M. Wasniowska, N. Janke-Gilman, W. Wulfhekel, M. Przybylski, and J. Kirschner, Surf. Sci. **601**, 3073 (2007).

[36] A. V. Davydenko, A. G. Kozlov, A. V. Ognev, M. E. Stebliy, A. S. Samardak, K. S. Ermakov, A. G. Kolesnikov, and L. A. Chebotkevich, Phys. Rev. B **95**, 064430 (2017).

[37] S. Zhang, J. Zhang, Q. Zhang, C. Barton, V. Neu, Y. Zhao, Z. Hou, Y. Wen, C. Gong, O. Kazakova, W. Wang, Y. Peng, D. A. Garanin, E. M. Chudnovsky, and X. Zhang, Appl. Phys. Lett. **112**, 132405 (2018).

[38] J. E. Davies, O. Hellwig, E. E. Fullerton, G. Denbeaux, J. B. Kortright, and K. Liu, Phys. Rev. B **70**, 224434 (2004).

[39] A. M. N. Niklasson, B. Johansson, and H. L. Skriver, Phys. Rev. B **59**, 6373 (1999).

[40] A. Michels, J. Weissmuller, A. Wiedenmann, J. A. Pedersen, and J. G. Barker, Philos. Mag. Lett. **80**, 785 (2000).

[41] M. Belmeguenai, M. S. Gabor, Y. Roussigne, T. Petrisor, R. B. Mos, A. Stashkevich, S. M. Cherif, and C. Tiusan, Phys. Rev. B **97**, 054425 (2018).

[42] A. Samardak, A. Kolesnikov, M. Stebliy, L. Chebotkevich, A. Sadovnikov, S. Nikitov, A. Talapatra, J. Mohanty, and A. Ognev, Appl. Phys. Lett. **112**, 192406 (2018).

[43] S. P. Vernon, S. M. Lindsay, and M. B. Stearns, Phys. Rev. B **29**, 4439 (1984).

[44] M. Grimsditch, E. E. Fullerton, and R. L. Stamps, Phys. Rev. B **56**, 2617 (1997).